PUBLICATIONS OF THE ASTRONOMICAL SOCIETY OF THE PACIFIC, **123**:1398–1411, 2011 December

Single-Dish Performance of KVN 21 m Radio Telescopes: Simultaneous Observations at 22 and 43 GHz

SANG-SUNG LEE,[1,2] DO-YOUNG BYUN,[1,2] CHUNG SIK OH,[1,2] SEOG-TAE HAN,[1,2] DO-HEUNG JE,[1] KEE-TAE KIM,[1,2] SEOG-OH WI,[1] SE-HYUNG CHO,[1,3] BONG WON SOHN,[1,2] JAEHEON KIM,[1,2,4] JEEWON LEE,[1,4] SE-JIN OH,[1] MIN-GYU SONG,[1] JIMAN KANG,[1] MOON-HEE CHUNG,[1] JEONG AE LEE,[1,5] JUNGHWAN OH,[1,2] JAE-HAN BAE,[1] SO-YOUNG YUN,[1] JUNG-WON LEE,[1] BONG GYU KIM,[1,2] HYUNSOO CHUNG,[1] DUK-GYOO ROH,[1] CHANG HOON LEE,[1] HYUN GOO KIM,[1] HYO RYOUNG KIM,[1] JAE-HWAN YEOM,[1] TOMOHARU KURAYAMA,[1] TAEHYUN JUNG,[1] PULUN PARK,[1,2] MIN JOONG KIM,[1,6] DONG-HWAN YOON,[1] AND WON-JU KIM[1,7]

Received 2011 September 2; accepted 2011 October 17; published 2011 November 8

ABSTRACT. We report simultaneous multifrequency observing performance at 22 and 43 GHz of the 21 m shaped-Cassegrain radio telescopes of the Korean VLBI Network (KVN). KVN is the first millimeter-dedicated VLBI network in Korea having a maximum baseline length of 480 km. It currently operates at 22 and 43 GHz and is planned to operate in four frequency bands: 22, 43, 86, and 129 GHz. The unique quasi optics of KVN enable simultaneous multifrequency observations based on efficient beam filtering and accurate antenna-beam alignment at 22 and 43 GHz. We found that the offset of the beams is within less than 5″ over all pointing directions of the antenna. The dual-polarization, cooled, high electron mobility transistor (HEMT) receivers at 22 and 43 GHz result in receiver noise temperatures less than 40 K at 21.25–23.25 GHz and 80 K at 42.11–44.11 GHz. The pointing accuracies have been measured to be 3″ in azimuth and elevation for all antennas. The measured aperture efficiencies are 65%(K)/67%(Q), 62%(K)/59%(Q), and 66%(K)/60%(Q) for the three KVN antennas, KVNYS, KVNUS, and KVNTN, respectively. The main-beam efficiencies are measured to be 50%(K)/52%(Q), 48%(K)/50%(Q), and 50%(K)/47%(Q) for KVNYS, KVNUS, and KVNTN, respectively. The estimated Moon efficiencies are 77%(K)/90%(Q), 74%(K)/79%(Q), and 80%(K)/86%(Q) for KVNYS, KVNUS, and KVNTN, respectively. The elevation dependence of the aperture efficiencies is quite flat for elevations greater than 20°.

Online material: color figures

1. INTRODUCTION

The Korean VLBI Network (KVN) is the first millimeter-dedicated very long baseline interferometry (VLBI) network in East Asia, aiming to study the formation and death of stars, the structure and dynamics of our own Galaxy, and the nature of active galactic nuclei (Kim et al. 2004; Wajima et al. 2005). Simultaneous multifrequency VLBI observations using the multifrequency band receiver systems (Han et al. 2008) will enable us to conduct observational studies with high spatial and temporal resolution based on the technique of multifrequency phase referencing (Asaki et al. 1998; Middelberg et al. 2005; Jung et al. 2011).

The KVN project was started in 2001 by the Korea Astronomy and Space Science Institute (KASI) with the construction of three 21 m radio telescopes in Seoul, Ulsan, and Jeju Island, Korea; KVN Yonsei Radio Telescope (KVNYS), KVN Ulsan Radio Telescope (KVNUS), and KVN Tanma Radio Telescope (KVNTN). The telescopes are located on the campuses of Yonsei University (Seoul), Ulsan University (Ulsan), and Tamna University (Jeju Island). KVN can operate simultaneously in two radio frequency bands, 22 and 43 GHz, and will be upgraded for simultaneous four-frequency observations, including the higher frequencies at 86 and 129 GHz. The maximum baseline length is ∼480 km and the maximum angular resolution at the highest operating frequency (129 GHz) is ∼1 mas.

[1] Korean VLBI Network, Korea Astronomy and Space Science Institute, P.O. Box 88, Yonsei University, Seongsan-ro 262, Seodaemun, Seoul 120-749, Republic of Korea; sslee@kasi.re.kr.

[2] Yonsei University Observatory, Yonsei University, Seongsan-ro 262, Seodaemun, Seoul 120-749, Republic of Korea.

[3] Department of Astronomy, Yonsei University, Seongsan-ro 262, Seodaemun, Seoul 120-749, Republic of Korea.

[4] Department of Astronomy and Space Science, Kyung Hee University, Seocheon-Dong, Giheung-Gu, Yongin, Gyeonggi-Do, 446-701.

[5] University of Science and Technology, 133 Gwahangno, Yuseong-gu, Daejeon, 305-333, Republic of Korea.

[6] Department of Astronomy and Space Science, Sejong University, Seoul 143-747, Korea.

[7] Department of Astronomy and Space Science, Chungnam National University, Daejeon 305-764, Korea.

A single-dish first light was received by the KVN Yonsei Radio Telescope on 2008 August 30. Following the single-dish performance-evaluation observations, all three radio telescopes of KVN are now operational and actively operated for single-dish observations of H_2O, SiO, and methanol maser sources and extragalactic compact radio sources (Kim et al. 2010). In this article we introduce the general aspects of the radio telescopes of the new millimeter-VLBI network and describe the results of the performance-evaluation observations. In § 2, we describe general aspects of observing systems of the Korean VLBI Network. We report the results of the performance-evaluation observations for the single-dish radio telescopes in § 3. In § 4, some astronomical results using KVN radio telescopes are described. Our results are summarized in § 5.

2. TELESCOPE SYSTEM

The KVN project aimed to build the first millimeter-dedicated VLBI network in Korea. KVN has a unique observing system, allowing simultaneous multifrequency single polarization observing in up to four frequency bands: 22, 43, 86, and 129 GHz or simultaneous multifrequency dual-polarization observing in two frequency bands out of four. A new millimeter-wave receiver optics system with three frequency-selective surfaces (dichroic filters) is an essential part of the unique system (Han et al. 2008). In this section we describe the main technical features of the KVN antennas and the observing system.

2.1. Antennas

The three 21 m antennas of KVN have been constructed by KASI under a contract with an American company, Antedo, Inc., and a Korean company, HighGain, from 2004 to 2008. The antennas are located at university campuses that have well-developed infrastructures and yield the optimal VLBI baselines for the Korean VLBI Network in the Korean peninsula. The main design features of the reflectors are determined by the fact that the antennas maintain a high surface accuracy of less than 150 μm rms and a pointing accuracy of less than 4″ at wind speeds of less than 10 m s^{-1}, and the aperture efficiency should be high enough (e.g., ~60% at 100 GHz) as a millimeter-dedicated VLBI network. The KVN antennas are therefore designed to be a shaped-Cassegrain-type antenna with an altitude-azimuth mount (Fig. 1). The telescope has a 21 m diameter main reflector with a focal length of 6.78 m. The main reflector consists of 200 aluminum panels with a manufacturing surface accuracy of ~65 μm. The slewing speed of the main reflector is 3° s^{-1}, which enables fast position-switching observations. The subreflector position, tilt, and tip are remotely controlled and modeled to compensate for the gravitational deformation of the main reflector and for the sagging-down of the subreflector itself. The characteristics of the antenna systems are summarized in Table 1.

FIG. 1.—Photograph of the 21 m diameter KVN Tamna radio telescope. See the electronic edition of the *PASP* for a color version of this figure.

TABLE 1
SPECIFICATION OF KVN ANTENNAS

Main Reflector (Axisymmetric Paraboloid)	
Diameter	$D = 21.03$ m
Focal length	$f = 6.78$ m
Focal ratio	$f/D = 0.32$
Panels manufacturing accuracy	65 μm
Alignment surface accuracy	50–54 μm
Subreflector (Hyperboloid)	
Diameter	$d = 2.25$ m
Manufacturing surface accuracy	50 μm
Expected total surface accuracy (EL ~ 48°[a]	124 μm
Panel	73 μm
Alignment	60 μm
Subreflector	52 μm
Backup structure	62 μm
Environmental Constraints	
Slewing speed	3° s^{-1}
Slewing acceleration	3° s^{-1}
Operating range	AZ: ± 270°, EL: 0°–90°

[a]Aggregate surface accuracy of KVN antennas obtained from root-sum-square calculation of measured and expected contributions by main reflector panels, alignment, subreflector, and antenna backup structures. Individual contribution includes measured accuracies, measurement errors, expected thermal, and wind effects.

2.2. Quasi Optics

A millimeter-wave receiver optics system with three frequency-selective surfaces (dichroic filters) is an essential component of the unique system, enabling simultaneous multi-frequency VLBI observations in four frequency bands, 22, 43, 86, and 129 GHz. The new receiver optics system has been described by Han et al. (2008), and only its salient features will be described in this section.

In order to make simultaneous observations in the four frequency bands, a receiver optics system was developed to split one signal into four using three low-pass filters with nominal cutoffs at 30, 70, and 108 GHz, made of multilayer metal meshes. The beam passing through the filter must have a large size. Furthermore, since each band is to provide dual-polarization observation, the receiver optics should generate as little cross-polarization as possible. As usual with shaped-Cassegrain antenna optics, the edge illumination at the subreflector by the receiver optics should be about 17 dB, i.e., less than 12 dB in conventional Cassegrain antenna optics, which leads to 2% spillover loss, resulting in higher illumination efficiency than obtainable from conventional Cassegrain optics fed with a scalar horn. Satisfying such requirements usually conflicts with physical space available inside an antenna cabin. The layout of the complete receiver optics is shown in Figure 2. This configuration was determined iteratively using standard quasi-optical theory (Goldsmith 1998), rather than computationally intensive physical optics method. The beam from the subreflector comes downward to the top of the 45° flat mirror. A microwave absorber may be inserted between the flat mirror and the first low-pass filter for system calibration based on the chopper-wheel method (Ulich & Haas 1976). The beam from the flat mirror may be reflected, pass through, or be filtered by three mode selectors, which consist of a flat mirror, a hole (or free space), and a low-pass filter (LPF). LPF1 (dichroic, cutoff ∼70 GHz) reflects the beam for the $86/129$ GHz branches and lets the beam for the $22/43$ GHz branches pass through. Likewise, LPF2 (cutoff ∼30 GHz) and LPF3 (cutoff ∼108 GHz) split beams into $22/43$ GHz and $86/129$ GHz, respectively. The 86 and 129 GHz receivers and their corresponding quasi-optical systems are currently being installed at three telescopes. Corrugated horns for 86 and 129 GHz are to be located inside cryogenic dewars, while horns for 22 and 43 GHz reside outside the respective dewars. The signal losses due to the dichroic filters were measured to be less than 2% (LPF1), less than 4% (LPF2), and less than 5% (LPF1 and LPF2) for the 22 GHz band and less than 2% (LPF1), less than 6% (LPF2), and less than 7% (LPF1 and LPF2) for the 43 GHz band (Table 2).

2.3. Receivers

The 22 and 43 GHz band signals separated in the quasi-optical system are coupled into the corrugated feed horns and receivers that have been built at KASI. The observing frequency bands for the receivers are 21.25–23.25 GHz and 42.11–44.11 GHz,

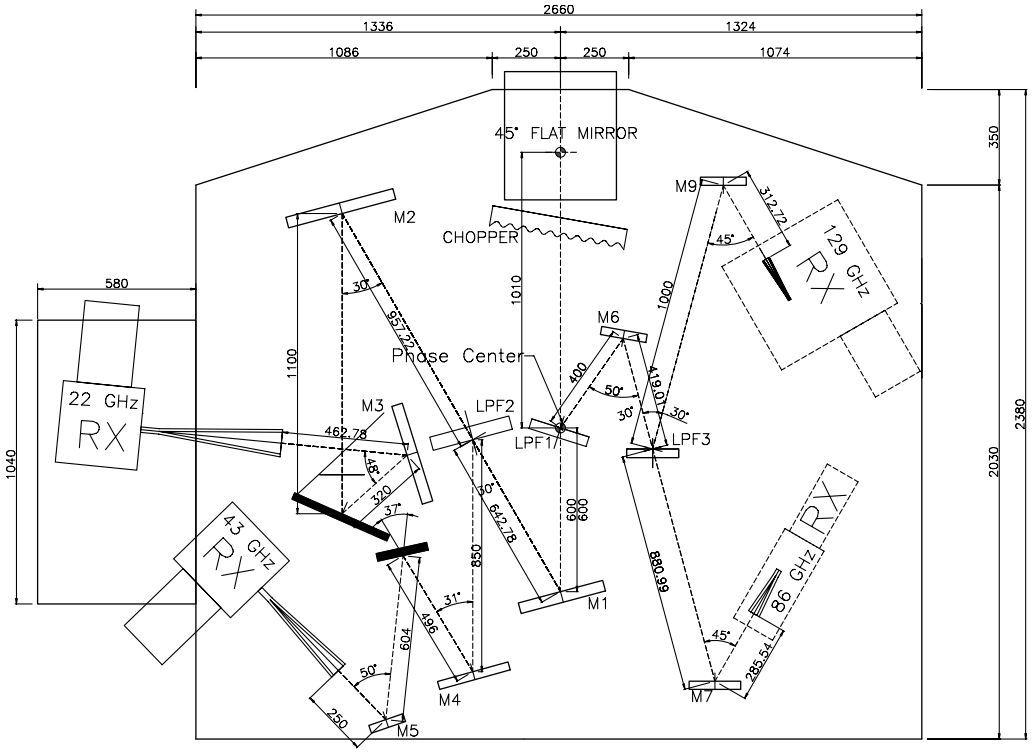

FIG. 2.—Layout of KVN receiver optics; top view, the beam from the antenna comes downward. The 86 and 129 GHz receivers and their corresponding quasi-optical systems (M6, M7, M8, and LPF3) are currently being installed. Dimensions are given in millimeters, and angles are in degrees.

TABLE 2
SIGNAL LOSSES BY DICHROIC FILTERS

Center freq. (GHz)	LPF1 LCP (%)	LPF1 RCP (%)	LPF2 LCP (%)	LPF2 RCP (%)	LPF1+LPF2 LCP (%)	LPF1+LPF2 RCP (%)
21.50	0.70	1.16	2.48	3.11	3.15	4.20
21.75	0.84	1.03	2.89	2.84	3.69	3.82
22.00	0.80	0.80	2.53	2.57	3.30	3.32
22.25	0.77	0.70	2.52	2.39	3.25	3.06
22.50	0.58	0.65	2.52	2.43	3.07	3.05
22.75	0.77	0.39	2.05	2.64	2.78	3.01
23.00	0.47	0.46	2.63	2.57	3.07	3.01
42.36	1.08	1.08	3.02	5.38	4.03	6.35
42.61	0.75	1.47	5.30	5.59	5.97	6.91
42.86	1.06	1.00	3.99	4.26	4.97	5.17
43.11	1.29	0.88	3.01	2.90	4.23	3.74
43.36	1.34	1.21	2.30	2.35	3.57	3.50
43.61	1.30	1.07	1.67	1.90	2.93	2.93
43.86	1.48	1.15	1.82	1.82	3.24	2.93

NOTE. —Frequency bandwidth for each measurement is 500 MHz. The measurements were done on 2008 July 17.

respectively. Both receivers are dual-circular-polarization, cooled HEMT receivers.

As shown in Figure 3, left-handed circular polarization and right-handed circular polarization components of the signals are separated in septum polarizers inside the dewar of each receiver. The InP HEMT amplifiers made by Caltech and NRAO are used as the first-stage low-noise amplifier for the 22 and 43 GHz receivers. The equivalent noise temperatures of both amplifiers are approximately 15 K over the whole observing frequency bands. The receiver noise temperatures for three 22 GHz receivers are measured to be 30–40 K. For the 43 GHz receivers, the receiver noise temperatures are 40–50 K for one receiver and 70–80 K for the other two receivers. The increase of the receiver noise temperatures results from the aggregated loss by feed horn, vacuum window, thermal isolator, and polarizer. The 43 GHz receiver with lower noise temperature is thermally isolated by a thermal isolator adopted at VLA, whereas the others are done by photonic bandgap isolators between dewar and polarizer. The spread of the receiver noise temperatures among 43 GHz receivers may be due to the difference of the thermal isolators. The signals are first amplified in a cooled stage and

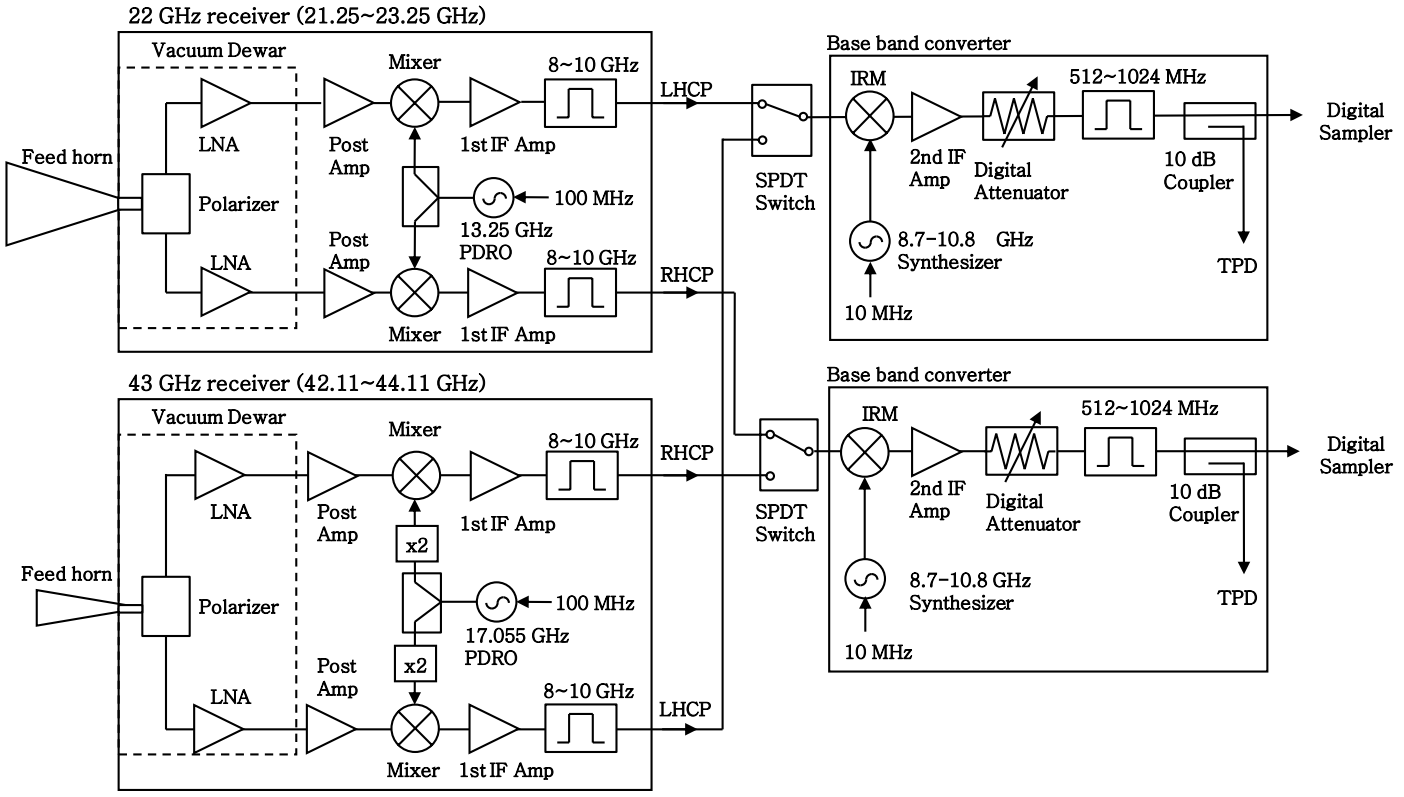

FIG. 3.—Simplified schematic diagram of 22 and 43 GHz receivers; The feed horn input signals are transmitted to the digital sampler and total power detector (TPD) through a LNA (low-noise amplifier), following a LNA, additional amplifications, two frequency conversions, and signal leveling. Two signals are selected using two single-pole/double-throw (SPDT) switches. PDRO: phase-locked dielectric resonator oscillator, x2: frequency doubler, LHCP: left-handed circular polarization, RHCP: right-handed circular polarization, and IRM: Image Rejection Mixer.

then further amplified by a room-temperature amplifier. They are then down-converted to 8–10 GHz, first IF (intermediate frequency) in the mixers using phase-locked dielectric resonator oscillators that are locked on the 100 MHz reference signal transmitted from the H-maser. The observing frequency bandwidth is limited within 2 GHz by bandpass filter) in the first IF. Two first-IF signals are selected using single-pole/double-throw switches. The selected signals may consist of single polarization signals at dual frequency bands or dual polarization signals at a single frequency band. The signal conditioning and second frequency conversion are done in the base band converter by using an image rejection mixer with an image rejection ratio of 18 dB, a 8.7–10.8 GHz frequency synthesizer with a step frequency of 100 Hz, and a digital step attenuator that offers an attenuation range up to 31.5 dB in steps of 0.5 dB. The final analog output signals are limited to 512–1024 MHz by an anti-aliasing filter.

2.4. Back Ends

The output signal from the base band converter is split into two different paths. One goes to a digital sampler and the other goes to a square-law detector (or total power detector). The output from the detector is amplified and input into a voltage-to-frequency converter (hereafter VFC). An embedded counter of the VFC counts the output pulse rates, which are proportional to the output power of the base band converter. The counted output pulse rates are taken every 100 ms by a receiver control computer in the receiver cabin. The VFC data are used not only for calibrating the receiver gain and the sky attenuation level, but also for measuring the total flux of celestial objects in continuum observation mode. An observing technique, cross scan, is used for the total flux measurements of pointlike objects in continuum single-dish observations at KVN. Since the technique relies on scanning with the main beam over the source position in both azimuth and elevation directions, the receiver gain and atmosphere fluctuations faster than a few seconds could not be tracked and removed. The calibration against the faster fluctuations will be improved by using a noise diode with known temperature and a faster data acquisition system.

The signals digitized by the samplers in the receiver room are processed by the KVN data acquisition system (DAS) to get spectra for single-dish spectroscopy observations. In VLBI operation, the digitized signals processed in the DAS are recorded onto storage media such as hard disks or magnetic tapes. As shown in Figure 4, the DAS consists of four subsystems; samplers, optical transmission system (OTS), digital filter bank (DFB), and digital spectrometer (DSM), which were manufactured by a Japanese company, Elecs Industry Company, Ltd. The samplers digitize base band signals into 2-bit data

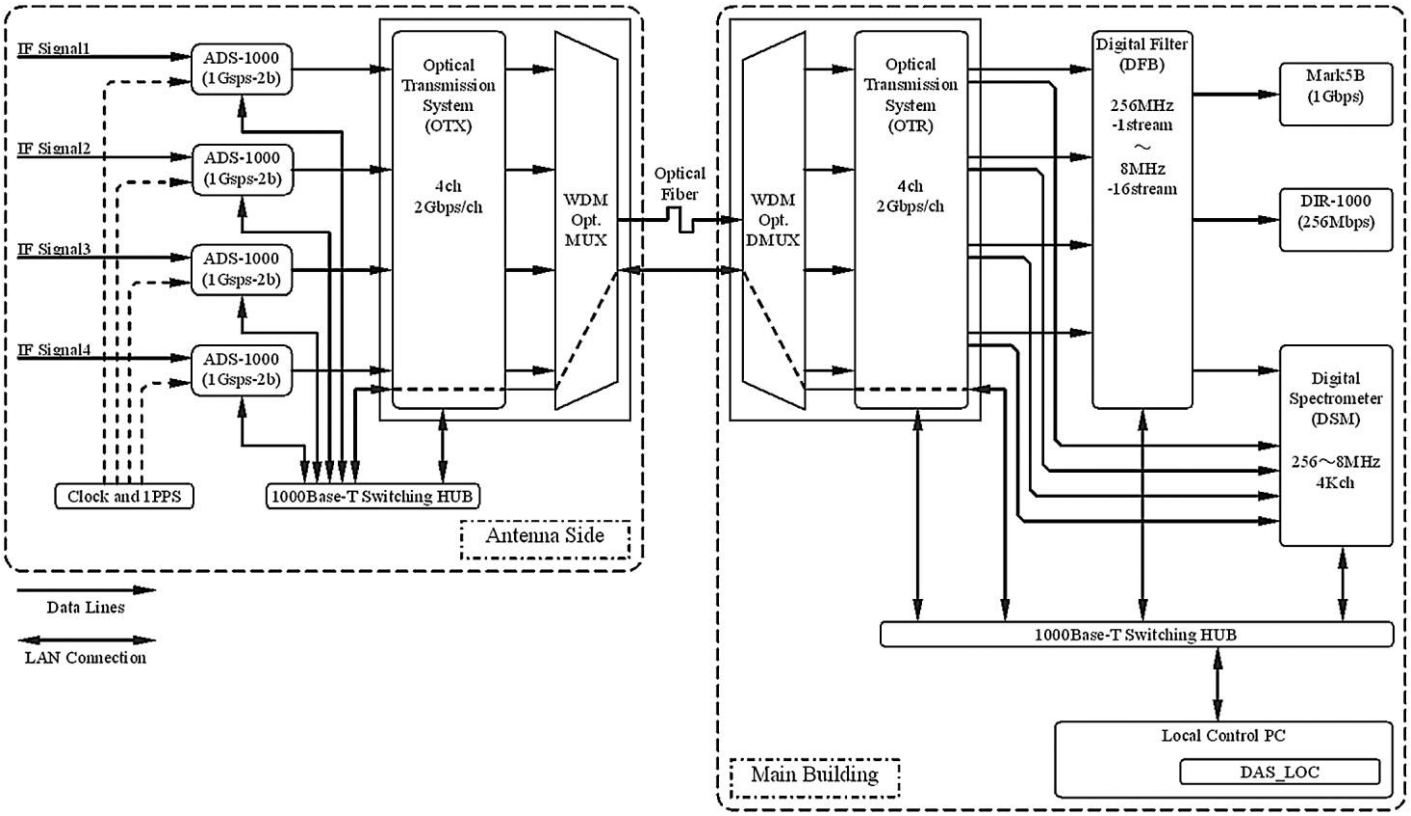

FIG. 4.—Schematic diagram of KVN data acquisition system. Adopted from Oh et al. (2011).

streams with four quantization levels. The output data streams of the samplers are transmitted to the observing building through optical fibers by the OTS. The DAS is configurable to various modes according to the required number of streams and bandwidths. For wideband observations, the DSM uses the output streams of the OTS, while for narrowband observations it uses the output stream of the DFB. In principle, the DFB produces 16 data streams of 16 MHz bandwidth from four streams of 512 MHz bandwidth. Combining more than one stream, the DFB can produce streams with wider bandwidths, such as 8×32 MHz, 4×64 MHz, 2×128 MHz, and 1×256 MHz. The DSM is a FX-type digital correlator, and we use the autocorrelation output for spectroscopy observations. Table 3 summarizes the available spectrometer outputs of the DSM. The correlation output produced by the DSM has 8192 channels, but the control computer can take only half of them. So we take full bandwidth after smoothing and binning pairs of adjacent channels, or half-bandwidth by selecting 4096 contiguous channels. For example, in the wide mode, we can get 4×512 MHz bandwidth spectra or 4×256 MHz bandwidth spectra. Detailed information for the KVN DAS is described in Oh et al. (2011). The DSM can calculate the cross-correlation of two input data streams and thus can be used for polarimetry. The polarimetry observation mode using a KVN single dish is currently being tested and will be described in a separate article.

2.5. Observation Control Software

For single-dish operation using a KVN antenna, we support various observation modes such as sky dipping, position-switching, frequency switching, focusing (FOCUS), five-point mapping (FIVE), grid mapping, cross scan (CS), and on-the-fly mapping (OTF). The observed data from all observing modes except for the continuum OTF mapping are stored into a Gildas CLASS file. The continuum OTF data written in ASCII format are reduced and converted into FITS format. The observation control software was written in Python programming language and runs on an IPython interpreter. A sequence of observations for many sources can be easily run by writing a simple Python script. The observation software runs on a PC running Linux. At most, eight streams of data can be simultaneously processed with a data-taking cycle of 100 ms. A graphical user interface is used for configuring devices and running observations.

TABLE 3
AVAILABLE DSM OUTPUTS

	Bandwidth[a] (MHz)	No. Streams
Wide Mode		
	512	4
Narrow Mode		
1	256	1
2	128	2
3	64	4
4	32	8
5	16	8
6	8	8
7	64/128	2/1
8	32/64/128	2/1/1
9	32/128	4/1
10	16/32/128	2/3/1

[a] Half-bandwidth can be taken with the same number of channels for all outputs.

3. PERFORMANCE TESTS

On 2008 October 10, we had first light with the KVN Yonsei radio telescope, simultaneously observing H_2O and SiO masers in Orion KL at 22 and 43 GHz. The resultant spectra at both frequency bands indicate that the overall receiving system of the KVN Yonsei radio telescope is functioning properly. In this section, we describe the results of single-dish performance tests for KVN radio telescopes.

3.1. Antenna Pointing Performance

3.1.1. Beam Alignment

It is very important to align the beams of different bands with each other as accurately as possible. Poor beam alignment will result in the large uncertainty of flux measurements for simultaneous multifrequency observations. Therefore, the beam alignment has to be measured and corrected to satisfy the requirement that two (or four) beams should be aligned within less than 10% of the FWHM of the smallest beam (e.g., 7″ for 22 and 43 GHz and 2.5″ for 22, 43, 86, and 129 GHz).

As a first step of the beam alignment measurements, we observed some bright and compact radio sources at 22 and 43 GHz, including planets and SiO maser sources, for measuring the beam alignment after the setup of the quasi optics. The beam alignments were estimated by measuring the pointing offsets at each frequency with CS and FIVE observing modes. If the measured beam alignments were larger than the requirement, we investigated the reasons for the poor alignment. For all cases, the poor beam alignments were caused by the misalignment of the quasi-optical system, including feed horns, and could be corrected by changing the angle of flat mirrors and feed horns in the quasi-optical system. Table 4 shows that the results of beam alignments with respect to the beam at 43 GHz for three KVN telescopes after corrections. The beams of all KVN antennas were very well aligned in azimuth, and there was no need for correction. However, beam offsets in elevation were measured to be as large as 7″. After changing the angle of flat mirrors in the quasi-optical system, we measured the beam offsets to be less than 5″. The elevation and azimuth dependence of the beam alignments have also been investigated by observing planets and SiO masers at various elevations. We found no significant elevation dependence of the beam alignments for all KVN antennas. This implies that the quasi-optical systems and

TABLE 4
MEASURED BEAM ALIGNMENTS OF KVN ANTENNAS AT 22 AND 43 GHZ

Epoch	Δ_{Az} (″)	Δ_{El} (″)	Source	Obs. mode
KVNYS				
2009 Sep	−2.3	+5.6	VX Sgr	FIVE
2009 Sep	−0.5	+4.2	Venus	CS
2009 Sep	−1.4	+4.6	Jupiter	CS
KVNUS				
2009 Sep	−4.2	+3.3	VX Sgr	FIVE
2009 Sep	−0.7	+3.3	Venus	CS
2009 Sep	−3.2	+2.9	Jupiter	CS
KVNTN				
2009 Dec	+1.3	−1.3	VX Sgr	FIVE
2009 Dec	+3.4	−4.3	Mars	CS
2009 Dec	+2.4	−1.8	Jupiter	CS

NOTE. —Offsets of the beam at 22 GHz measured with respect to the beam at 43 GHz.

the receiver plates, including the subplate for the 22 GHz receivers, are stable against gravitational deformation.

3.1.2. Pointing Accuracy

Since the beams at 22 and 43 GHz are well aligned with each other, it is efficient to establish the pointing model only at 43 GHz using SiO maser sources (mostly late-type stars) whose positions are very well known. As long as the alignment between two antenna beams is accurate to less than 10% of the FWHM at 43 GHz, the pointing model derived from SiO maser observations at 43 GHz should ensure the pointing accuracies for both frequency bands.

A pointing model had already been obtained by observing strong SiO maser sources with a 100 GHz receiving system. These observations had been done to evaluate the performance of the antenna under the contract with the antenna manufacturer (see Kim et al. 2011). On the basis of this pointing model established at 100 GHz, a sample of nine late-type stars (Table 5)

TABLE 5
SIO MASER SOURCES USED FOR POINTING MODEL

Source	α_{2000} (hh mm ss)	δ_{2000} (dd mm ss)	V_{LSR} (km/s)
R Cas	23 58 24.79	+51 23 19.5	+25.0
U Her	16 25 47.48	+18 53 33.0	−15.0
R Leo	09 47 33.49	+11 25 44.0	−1.0
IK Tau	03 53 28.87	+11 24 21.7	+37.1
o Cet	02 19 20.79	−02 58 37.4	+50.2
R Aqr	23 43 49.44	−15 17 03.9	+22.0
VX Sgr	18 08 04.05	−22 13 26.6	+5.7
W Hya	13 49 02.03	−28 22 03.0	+42.0
VY CMa	07 22 58.33	−25 46 03.2	+18.0

has been used continuously to improve the pointing accuracy of the telescope. Table 6 describes the accuracies of pointing models established for three KVN radio telescopes during the evaluation period of 2009–2011. The root mean square (rms) of the residual pointing offsets between the observations and the pointing models is listed in azimuth (σ_{Az}), elevation (σ_{El}), and total ($\sigma_{tot} = \sqrt{\sigma_{Az}^2 + \sigma_{El}^2}$), respectively, for each epoch and telescope (see Fig. 5 for an example of residual pointing offsets). Before applying a cladding system, the residual rms errors are less than 3″ in azimuth and less than 6″ in elevation. The pointing accuracies have been improved to be less than 3″ in both azimuth and elevation after applying the cladding system for more efficiently insulating the antenna mount structure.

Thermal deflection of the antenna mounting structures (yoke arms) have been investigated in order to improve the antenna pointing accuracy. When the antenna mounting structures face directly to the Sun, thermal deflection causes the antenna pointing offsets to rapidly change from a few to ∼40″ within an hour. The large pointing offsets result in a large uncertainty of flux measurements not only for single-dish observations, but also for VLBI (phase referencing) observations during daytime. Therefore, we decided to apply a cladding system to the antenna mounting structures (Fig. 6). The new cladding system provides an efficient thermal insulation by making an air gap with its thickness of 80 mm between the new and old cladding systems. New cladding systems were installed on 2010 October 14, 2010 November 6, and 2010 November 24 for KVNYS, KVNUS, and KVNTN, respectively. After applying the cladding, the pointing offsets due to thermal effects were reduced to be less than 20″ and the timescale of the thermal effects was improved to be greater than 5 hr. As a result, the rms residuals in the pointing model have been improved by a factor of ∼2 (Table 6). In the case of observations during daytime, especially at sunrise, the

TABLE 6
POINTING ACCURACIES OF KVN ANTENNAS AT 43 GHZ

Epoch	σ_{Az} (″)	σ_{El} (″)	σ_{tot} (″)
KVNYS			
2009 Mar 6	2.2	4.0	4.6
2009 Sep 18	2.2	5.0	5.5
2010 Oct 16[a]	1.7	2.6	3.1
KVNUS			
2009 Sep 9	2.9	4.9	5.7
2010 Oct 8	2.2	5.5	5.9
2010 Nov 8[a]	2.8	2.3	3.6
KVNTN			
2009 Dec 7	2.4	5.3	5.8
2010 Sep 17	2.6	5.7	6.3
2011 Jan 10[a]	2.0	2.8	3.4

[a]Pointing models established after improving the pointing accuracies by applying a cladding system.

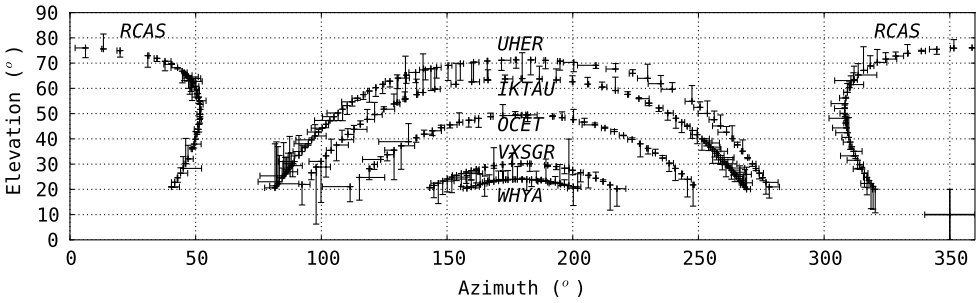

FIG. 5.—Residual pointing offsets of the pointing model for KVNYS established on 2010 October 16 through observations of six SiO maser sources. Cross in the lower right corner indicates the scale of error bars at 10″ in both azimuth and elevation.

pointing observations must be conducted out at least every hour for maintaining the pointing accuracy to be less than 4″.

3.2. Antenna Efficiency and Gain Curve

3.2.1. Antenna Efficiency

Surface accuracies of the main reflectors of the KVN radio telescopes had been measured by photogrammetry at an elevation of 48°, yielding alignment surface accuracies of 50, 54, and 51 μm for the KVN Yonsei, Ulsan, and Tamna telescopes, respectively (Kim et al. 2011). The expected total surface accuracy of KVN antennas is ~124 μm (Table 1), which is good to enable observations at frequencies of less than 150 GHz. The surface accuracies have been verified by the 100 GHz test observations, yielding aperture efficiencies of 52% and main-beam efficiencies of 46% for all three telescopes (Kim et al. 2011).

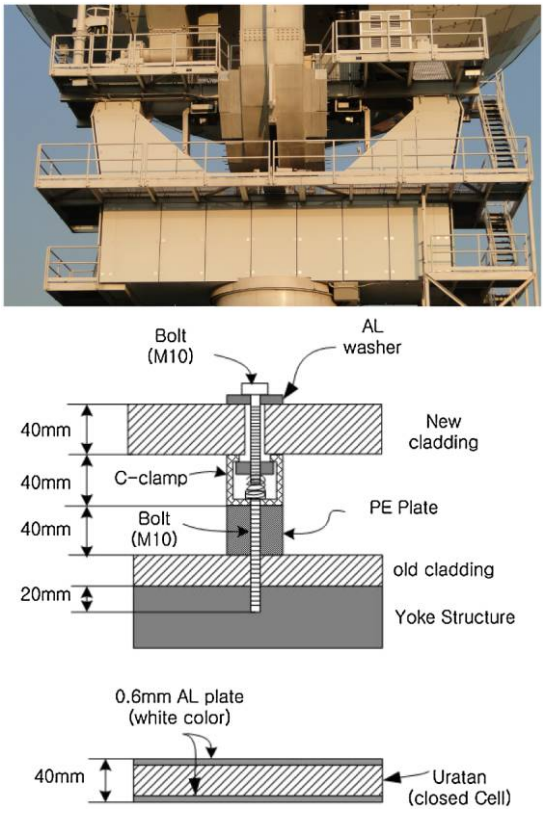

FIG. 6.—Antenna mounting structure (yoke arms) with new cladding system (*top*) and detailed structures of new cladding system (*bottom*). See the electronic edition of the *PASP* for a color version of this figure.

Since new receivers and quasi-optical systems at 22 and 43 GHz have been installed for KVN radio telescopes, the corresponding antenna efficiencies should be measured in order to evaluate the alignment of the quasi-optical systems including feed horns. The antenna efficiencies can be measured by observing primary calibrators such as planets. Since a planet can be considered as a disk with uniform brightness, the measured antenna temperature ($T_{\rm A}^{*}$) is related to the aperture ($\eta_{\rm A}$) and beam ($\eta_{\rm B}$) efficiencies as (Schloerb & Snell 1980; Rho & Jung 1999; Koo et al. 2003; Kim et al. 2011)

$$\eta_{\rm A} \equiv \frac{A_{\rm e}}{A_{\rm p}} = \frac{\lambda^2 T_{\rm A}^{*}}{A_{\rm p} T_{\rm B} \Omega_{\rm s}}, \tag{1}$$

$$\eta_{\rm B} \equiv \frac{\Omega_{\rm M}}{\Omega_{\rm A}} = \frac{T_{\rm A}^{*} \Omega_{\rm M}}{T_{\rm B} \Omega_{\rm s}} = \frac{A_{\rm p} \Omega_{\rm M}}{\lambda^2} \eta_{\rm A}, \tag{2}$$

$$\Omega_{\rm s} = \Omega_{\rm M} \left[1 - \exp\left(- \ln 2 \left(\frac{\theta_{\rm s}}{\theta_{\rm M}} \right)^2 \right) \right], \tag{3}$$

$$\Omega_{\rm M} = 1.133 \theta_{\rm M}^2, \tag{4}$$

where $A_{\rm e}$, $A_{\rm p}$, λ, $T_{\rm B}$, and $\Omega_{\rm s}$ are the effective and physical areas of main reflector, the observing wavelength, the brightness temperature, and the source solid angle, and $\Omega_{\rm M}$, $\Omega_{\rm A}$, $\theta_{\rm s}$, and $\theta_{\rm M}$ are the main-beam solid angle, the antenna solid angle, the angular size of the source, and the size of the main beam (FWHM), respectively.

Table 7 lists measurements of main-beam size, $\theta_{\rm M}$, aperture efficiency, $\eta_{\rm A}$, and main-beam efficiency, $\eta_{\rm B}$ at 22 and 43 GHz over the period from 2009 April to 2011 March. The measured

aperture efficiencies are 65%(K)/67%(Q), 62%(K)/59%(Q), and 66%(K)/60%(Q) for KVNYS, KVNUS, and KVNTN, respectively. The measurement errors of the aperture efficiencies are less than 2%. Main-beam sizes were estimated from the CS or OTF observations of Venus or Jupiter, as well as from the FIVE observations of strong H_2O and SiO maser sources. For each measurement of the aperture efficiency, Jupiter or Venus have been observed in CS or OTF mapping mode over various elevations when the angular sizes of the planets were smaller than the main-beam size at 43 GHz. Measurements at elevations of $\geq 30°$ were averaged to estimate the main-beam size and the aperture efficiency with their standard deviations listed in Table 7. The main-beam efficiency was calculated through its relation to the aperture efficiency (eq. [2]).

The uncertainties of the brightness temperatures of Venus (505 ± 25 K at the K band [Butler et al. 2001] and 450 ± 32 K at the Q band [Greve et al. 1994]) and Jupiter (134 ± 4 K at the K band [Page et al. 2003] and 150 ± 12 K at the Q band [Greve et al. 1994]) dominate the error of the aperture efficiency. The predicted aperture efficiencies from the original design of the antenna with a blockage efficiency of 88% are 72% at the K band and 75% at the Q band. The measured aperture efficiencies are lower than these by $\leq 10\%$ and $\leq 16\%$ at each band. This is, in fact, expected from the results of the 100 GHz test observations of the KVN radio telescopes (Kim et al. 2011). The 100 GHz aperture efficiencies are 52% for the three antennas, which are lower than the designed value of 60%, due to a slightly lower blockage efficiency from the additional cladding of the subreflector supports. The aperture efficiencies at 100 GHz are similar for all antennas, whereas those at K and Q bands are different for each antenna. At the K band, the aperture efficiency of KVNUS is lower than those of the others, and at the Q band, KVNUS and KVNTN have lower aperture efficiencies than KVNYS. This may be because of larger misalignment of the quasi-optical system at KVNUS and KVNTN than that at KVNYS. The aperture efficiency is degraded if the quasi-optical system is not well aligned with the antenna, although the relative beam alignment between the two frequency bands is good. The alignment will be improved when new receivers at 86 and 129 GHz and corresponding quasi-optical systems are installed.

The measured main-beam sizes are $122''(\mathrm{K})/64''(\mathrm{Q})$, $123''(\mathrm{K})/66''(\mathrm{Q})$, and $124''(\mathrm{K})/64''(\mathrm{Q})$ for KVNYS, KVNUS, and KVNTN, respectively, over the period from 2009 April to 2011 March (Table 7). The main-beam sizes have no dependence on elevation and a small difference of less than 4% between azimuth and elevation directions. These main-beam sizes are smaller by ~10% than the diffraction limit of 135″ at

TABLE 7

EFFICIENCIES OF KVN ANTENNAS AT 22 AND 43 GHZ

Band	Epoch	θ_M (″)	η_A (%)	η_B (%)	Target	Ang. size (″)	Elevation (°)
KVNYS							
K	2009 Apr 7	124.6 ± 0.6	71.9 ± 1.2	56.6	Venus	56.1	30-59
Q	2009 Apr 8	65.1 ± 2.4	68.5 ± 0.8	55.3	Venus	55.5	30-59
K	2010 Nov 10	123.4 ± 1.2	61.4 ± 0.5	47.4	Jupiter	45.8	30-49
Q	2010 Nov 11	66.8 ± 0.6	64.3 ± 0.4	54.8	Jupiter	45.7	30-49
K	2011 Mar 16	120.9 ± 1.1	66.6 ± 0.8	49.4	Venus	14.4	30-34
Q	2011 Mar 16	62.1 ± 0.6	67.3 ± 1.0	49.5	Venus	14.4	30-34
K	2011 Mar 16	120.5 ± 1.7	61.5 ± 0.8	45.3	Jupiter	33.4	30-56
Q	2011 Mar 16	61.5 ± 0.9	67.7 ± 1.0	48.9	Jupiter	33.4	30-56
KVNUS							
K	2009 Sep 17	124.4 ± 3.3	64.5 ± 1.9	50.6	Venus	11.8	30-59
Q	2009 Sep 18	65.9 ± 3.9	67.6 ± 0.7	56.0	Venus	11.7	30-59
K	2010 Nov 10	124.0 ± 0.3	60.2 ± 0.5	47.0	Jupiter	45.8	30-50
Q	2010 Nov 10	68.2 ± 0.2	56.3 ± 0.9	50.0	Jupiter	45.8	30-50
K	2011 Mar 16	121.5 ± 0.9	64.6 ± 0.6	48.4	Venus	14.4	30-39
Q	2011 Mar 16	64.3 ± 0.7	57.1 ± 0.8	45.0	Venus	14.4	30-39
K	2011 Mar 16	122.9 ± 1.0	60.1 ± 0.3	46.1	Jupiter	33.4	30-58
Q	2011 Mar 16	66.1 ± 0.6	56.9 ± 1.1	47.4	Jupiter	33.4	45-53
KVNTN							
K	2011 Feb 15	121.4 ± 0.8	69.4 ± 0.4	51.9	Venus	17.5	30-35
Q	2011 Feb 15	63.3 ± 0.3	60.3 ± 0.4	46.1	Venus	17.5	30-35
K	2011 Feb 15	122.8 ± 0.6	63.4 ± 0.4	48.5	Jupiter	34.7	30-57
Q	2011 Feb 15	65.3 ± 0.4	59.5 ± 1.4	48.4	Jupiter	34.7	30-57

NOTE. —The brightness temperatures used of Jupiter/Venus are 134 ± 4 K (Page et al. 2003)/505 ± 25 K (Butler et al. 2001) at the K band and 150 ± 12 K (Greve et al. 1994)/450 ± 32 K (Greve et al. 1994) at the Q band. The uncertainties of the main-beam size and the aperture efficiency include only statistical measurement errors.

22.235 GHz and 70″ at 43.122 GHz for uniform aperture illumination. This may result from blockage effect (Heiles et al. 2001) and/or inverse-tapered illumination of the main reflector. These effects also result in relatively higher sidelobe levels than for the conventional Cassegrain antenna. The antenna-beam patterns for all KVN antennas were measured and the beam pattern for KVNTN is shown in Figure 7. The first sidelobe levels are -13.0 dB/-13.0 dB (K/Q), -13.0 dB/-12.7 dB (K/Q), and -13.1 dB/-12.7 dB (K/Q) for KVNYS, KVNUS, and KVNTN, respectively. The measured sidelobe levels are significantly higher than those (-17.6 dB) for the Cassegrain antennas with uniform illumination pattern and without blockage (Rohlfs & Wilson 2000). It should be noticed that, due to the higher sidelobe level, spectral line observation data should be carefully analyzed, taking into account possible coupling to the first sidelobe.

The main-beam efficiencies are measured to be 50%(K)/52%(Q), 48%(K)/50%(Q), and 50%(K)/47%(Q) for KVNYS, KVNUS, and KVNTN, respectively. Since the main-beam efficiency was estimated according to its relation to the aperture efficiency (eq. [2]), the statistical errors are not estimated. However, the estimation of the main-beam efficiencies are also affected by the uncertainty of the brightness temperatures of Venus and Jupiter and the measurement errors of main-beam sizes. Due to the high-level sidelobes, the main-beam efficiencies are lower with respect to the aperture efficiencies than in the case of conventional Cassegrain telescopes.

We measured Moon efficiencies, $\eta_{\rm Moon}$, of the KVN radio telescopes by OTF mapping of the Moon at 22 and 43 GHz. The Moon efficiencies were derived based on Linsky (1973) and Mangum (1993). The estimated Moon efficiencies are 77%(K)/90%(Q), 74%(K)/79%(Q), and 80%(K)/86%(Q) for KVNYS, KVNUS, and KVNTN, respectively (Table 8).

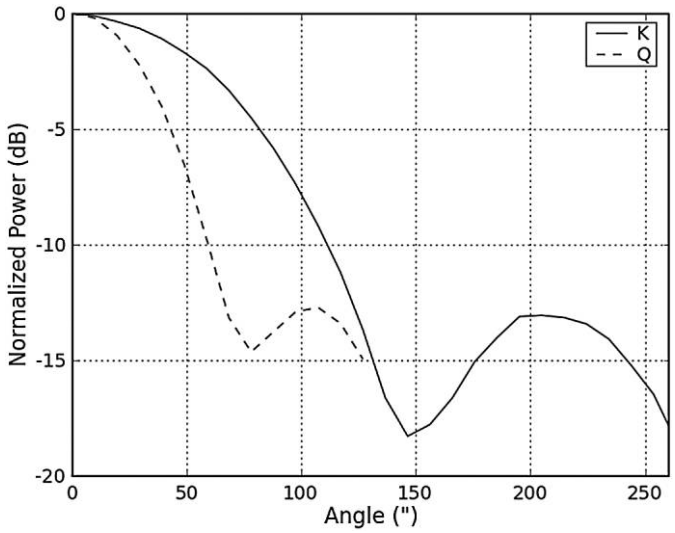

FIG. 7.—Azimuthally averaged beam patterns at the K band (*solid line*) and Q-band (*dashed line*) for KVNTN from OTF mapping observations of Jupiter.

TABLE 8

MOON EFFICIENCIES OF KVN ANTENNAS AT 22 AND 43 GHZ

Band	Epoch	UT (hh:mm)	Phase (days)	$T_{\rm a}^{*}$ (K)	$\eta_{\rm moon}$ (%)
KVNYS					
K	2011 Mar 15	18:30	10.5	184.1	76.9
Q	2011 Mar 15	18:30	10.5	215.0	89.6
KVNUS					
K	2011 Mar 16	19:20	11.5	181.7	73.6
Q	2011 Mar 16	19:20	11.5	198.8	78.8
KVNTN					
K	2011 Feb 15	12:50	12.4	202.0	79.8
Q	2011 Feb 15	12:50	12.4	224.6	85.7

NOTE. —We used 239 K and 234 K at K and Q bands for the brightness temperatures of Moon based on Linsky (1973).

The error of the Moon efficiency is dominated by the measurement error of the antenna temperature of the Moon, which is as large as 1–2%.

3.2.2. Gain Curve

Gain-curve measurements were made in 2009 September for KVN Yonsei, in 2011 March for KVN Ulsan, and in 2010 December for KVN Tamna. The elevation dependence of the aperture efficiency of the KVN 21 m radio telescopes was measured by observing bright H_2O and SiO maser sources at 22 and 43 GHz in dual polarizations (LCP and RCP) using the FIVE pointing observations. Every 10 FIVE pointing observations, the atmospheric opacity was measured and the subreflector focus was adjusted based on the preestablished model for the subreflector. In order to avoid gain degradation due to the thermal deformation of the antenna, the gain-curve measurements were performed at night.

The pointing offsets were corrected during the data reduction based on the results of the FIVE pointing observations. Figure 8 shows the normalized spectral line intensities of H_2O and SiO maser sources in elevations of 10°–70° for KVN Yonsei, Ulsan, and Tamna at 22 and 43 GHz. A second-order polynomial was least-squares-fitted to the data. The fitted function was normalized by its maximum. Normalized gain curve has the following form: $\mathrm{Gain_{norm}} = \mathrm{A0} \times \mathrm{El}^2 + \mathrm{A1} \times \mathrm{El} + \mathrm{A2}$, where El is the elevation in degrees. The fitted parameters are summarized in Table 9. The gain curves at 22 GHz are quite flat at the elevations of greater than 20°. At 43 GHz, the antenna gains at low elevation decrease by less than 10%.

4. SOME ASTRONOMICAL RESULTS

4.1. Maser Line Surveys of the Galactic Star-forming Regions

Extensive simultaneous H_2O $6_{16} - 5_{23}$ (22.23508 GHz) and CH_3OH $7_0 - 6_1$ A^+ (44.06943 GHz) maser line surveys were carried out on Galactic young stellar objects (YSOs) using the

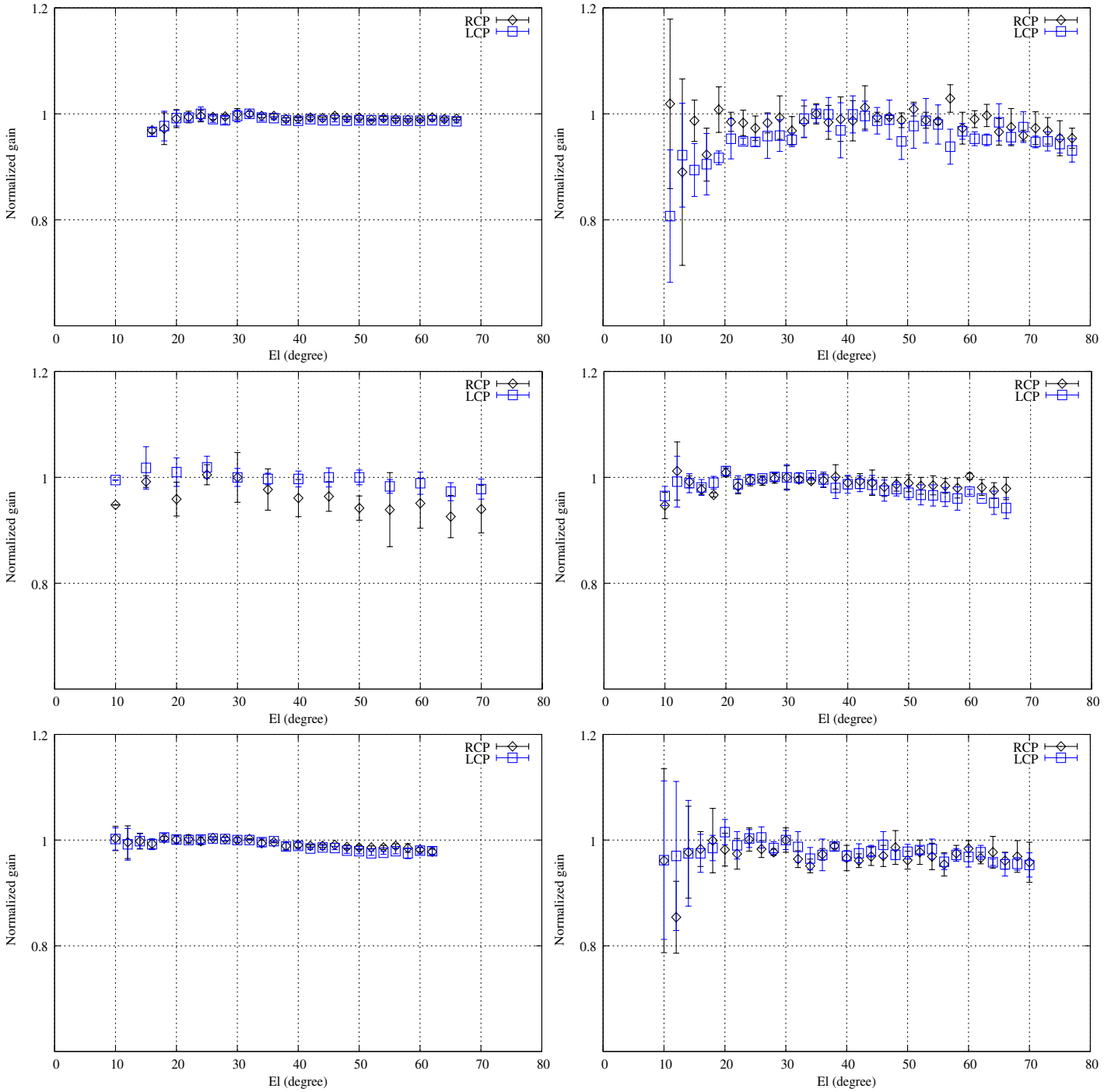

FIG. 8.—Gain curves of KVN Yonsei (top), Ulsan (*middle*), and Tamna (*bottom*) at 22 GHz (*left*) and 43 GHz (*right*). See the electronic edition of the *PASP* for a color version of this figure.

KVN 21 m telescopes. Because of variability of the two masers, simultaneous observations are important for comparison of their properties in detail. Bae et al. (2011) report the observational results on 180 intermediate-mass YSOs, including 14 Class 0 objects, 19 Class I objects, and 147 Herbig Ae/Be stars that are widely believed to be intermediate-mass stars in the pre-main-sequence phase. H_2O and CH_3OH maser emissions were detected for 16 (9%) and 10 (6%) sources, respectively. The detection rates of both masers rapidly decrease as the central (proto) stars evolve, which is consistent with the trend for H_2O

TABLE 9
NORMALIZED GAIN-CURVE PARAMETERS OF KVN ANTENNAS AT 22 AND 43 GHZ

Band	Epoch	A0	A1	A2
KVNYS				
K	2009 Sep	-6.70130×10^{-6}	$+4.85791 \times 10^{-4}$	0.991196
Q	2009 Sep	-3.94673×10^{-5}	$+3.47852 \times 10^{-3}$	0.923354
KVNUS				
K	2011 Mar	-1.39267×10^{-6}	-5.56796×10^{-4}	1.005707
Q	2011 Mar	-1.94371×10^{-5}	$+1.41639 \times 10^{-3}$	0.974197
KVNTN				
K	2009 Dec	-1.35247×10^{-5}	$+6.81293 \times 10^{-4}$	0.991420
Q	2009 Dec	-1.91393×10^{-5}	$+1.23772 \times 10^{-3}$	0.979990

masers observed in low-mass star-forming regions (Furuya et al. 2001). This indicates that the excitation of the two masers is related to the evolutionary stage of the central object. H_2O masers usually have significantly larger relative velocities with respective to the ambient molecular gas than do CH_3OH masers. The isotropic luminosities of both masers are well correlated with the bolometric luminosities of the central (proto) stars.

The same maser line surveys were performed of more than 1000 high-mass YSOs in different evolutionary phases: infrared dark cores, high-mass protostellar candidates, and ultracompact H II regions (Kim et al. 2011, in preparation). The detection rates of both masers significantly increase as the central objects evolve. This is contrary to the trends found in low- and intermediate-mass star-forming regions, as mentioned previously. Thus, the excitation of the two masers appears to be closely related to the circumstellar environments, as well as to the evolutionary stage of the central (proto) stars.

4.2. Late-Type Stars

Studies of late-type stars using the KVN Yonsei radio telescope were performed of known stellar SiO and/or H_2O maser sources (166 SiO-and-H_2O maser sources, 83 SiO-only sources, and 152 H_2O-only sources) soon after finishing the performance test observations. Both SiO and H_2O masers were detected from 112 sources at one epoch, giving a detection rate of 67% for 166 SiO-and-H_2O maser sources (Kim et al. 2010); detected from 14 sources (detection rate of 17%) for 83 SiO-only sources (Cho et al. 2011 in preparation); and detected from 62 sources (detection rate of 41%) for 152 H_2O-only sources (Kim et al. 2011, in preparation). Some spectra simultaneously obtained in the H_2O $6_{16} - 5_{23}$ and SiO $v = 1$ and 2, $J = 1 - 0$ transitions are shown in Figure 9. Through simultaneous observations of SiO and H_2O masers, relations between SiO and H_2O maser properties and the dynamical connection from the pulsating atmosphere to the inner circumstellar envelope were investigated for evolved stars. The distributions of single- and double-peaked profiles of H_2O maser lines were also examined in the IRAS two-color diagram. These single- and double-peaked H_2O maser lines can be associated with an asymmetric wind and bipolar outflows, which are commonly seen in protoplanetary nebulae and planetary nebulae, as suggested by Engels (2002).

4.3. Intraday Variable Source 0716 + 714

Total flux monitoring of the intraday variable source $0716 + 714$ was made simultaneously at 21.7 GHz and 42.4 GHz with the KVN Yonsei 21 m radio telescope on 2009 December 11–15 and 2010 January 4–11. An absolute calibrator, 3C 286, was observed for flux calibration, and a nearby secondary calibrator,

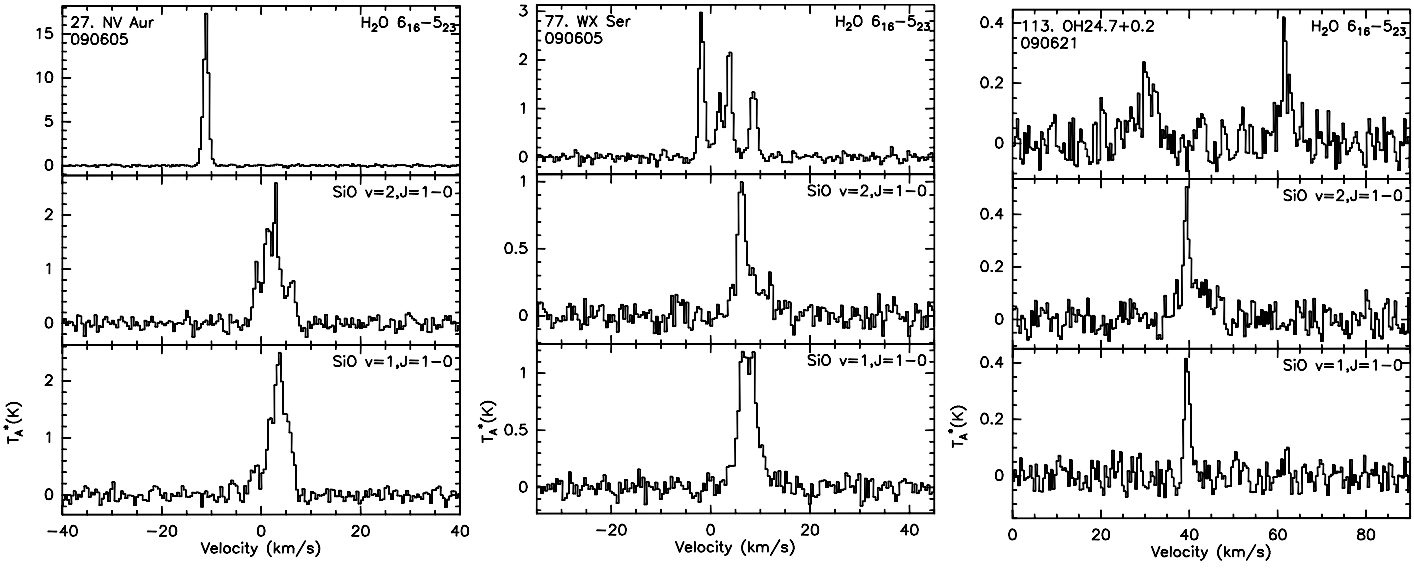

FIG. 9.—Sample spectra of three late-type stars (NV Aur, WX Ser, and OH24.7 + 0.2) simultaneously obtained in the H_2O $6_{16} - 5_{23}$ and SiO $v = 1$ and 2, $J = 1 - 0$ transitions. Adopted from Kim et al. (2010).

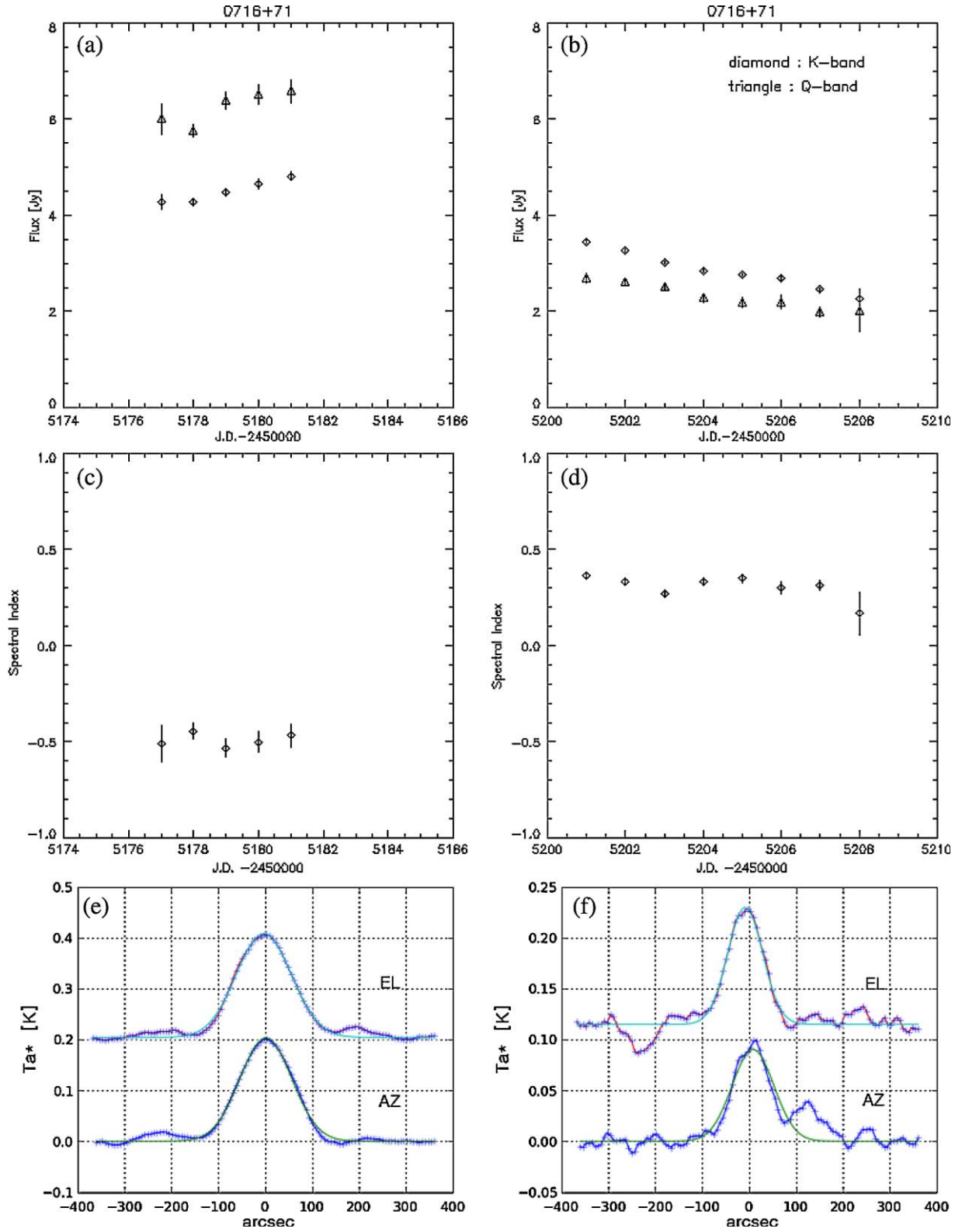

FIG. 10.—Light curves of 0716 + 714 in (*a*) 2009 December (JD 24505177–24505181) and (*b*) 2010 January (JD 24505201–24505208) and spectral indices for the measurements in (*c*) 2009 December and (*d*) 2010 January. Examples of cross-scan profiles with their Gaussian fits of a flux calibrator 3C 286 taken simultaneously at (*e*) 21.7 GHz and (*f*) 42.4 GHz. Error bars (1σ) in (*a*)–(*d*) are statistical only. Effective on-source integration times for the examples (*e*) and (*f*) are 40 and 20 s, respectively. See the electronic edition of the *PASP* for a color version of this figure.

$0836+714$, observed for gain calibration. All flux measurements were done with CS mode. The total bandwidth was 500 MHz at both frequency bands. Figure 10 shows the light curves and spectral indices of $0716+714$ for two epochs. In these observations, intraday variability of $0716+714$ is not seen, but a monotonic increase and decrease of total flux density on longer timescales were observed. More interestingly, as the source gets brighter, the spectral index becomes flatter, and vice versa.

5. SUMMARY

Through the performance-evaluation observations in 2008–2011, we found that the KVN 21 m radio telescopes are suitable for simultaneous multifrequency single polarization observations at 22 and 43 GHz. The dual beams at two frequencies are well aligned within less than 5″. The pointing accuracies are less than 3″ in azimuth and elevation. The measured aperture efficiencies are greater than 64% at 22 GHz and greater than 62% at 43 GHz, the main-beam efficiencies are greater than 49% at 22 GHz and greater than 50% at 43 GHz, and the estimated Moon efficiencies are greater than 77 at 22 GHz and greater than 85% at 43 GHz. The elevation dependence of the aperture efficiencies is quite flat at the elevations of greater than 20° Unique receiving systems, accurate beam alignment, and high antenna efficiencies will provide us with good opportunities for scientific observations at millimeter wavelengths, not only for single radio telescope, but also for very long baseline interferometry.

Further instrumentation for KVN will include 86 and 129 GHz receivers, which should be ready in late 2012. Simultaneous four-frequency observations will be ready for VLBI observations.

This work was supported by a Basic Research Program (2008–2011) and also partially supported by a Korea Astronomy and Space Science Institute (KASI)-Yonsei Joint Research Program (2010–2011) for the Frontiers of Astronomy and Space Science funded by the Korea Astronomy and Space Science Institute. We are grateful to Paul Goldsmith for careful reading of and kind comments for the manuscript. We would like to thank the anonymous referee for providing prompt and thoughtful comments that helped improve the original manuscript. S. S. L. and B. W. S. were partially supported by a Korea-EU FP7 RadioNet program funded by National Research Foundation of Korea (NRF). M. K. was supported by a Basic Science Research Program through the NRF, funded by the Ministry of Education, Science and Technology (2009-0066892).

REFERENCES

Asaki, Y., Shibata, K. M., Kawabe, R., Roh, D.-G., Saito, M., Morita, K.-I., & Sasao, T. 1998, Radio Sci., 33, 1297

Bae, J.-H., Kim, K.-T., Youn, S.-Y., Kim, W.-J., Byun, D.-Y., Kang, H., & Oh, C. S. 2011, ApJS, 196, 21

Butler, B. J., Steffes, P. G., Suleiman, S. H., Kolodner, M. A., & Jenkins, J. M. 2001, Icarus, 154, 226

Engels, D. 2002, A&A, 388, 252

Furuya, R. S., Kitamura, Y., Wootten, H. A., Claussen, M. J., & Kawabe, R. 2001, ApJ, 559, L 143

Goldsmith, P. F. 1998, Quasioptical Systems: Gaussian Beam Quasioptical Propagation and Applications (New York: IEEE)

Greve, A., Steppe, H., Graham, D., & Schalinski, C. J. 1994, A&A, 286, 654

Han, S.-T., Lee, J.-W., Kang, J., Je, D.-H., Chung, M.-H., Wi, S.-O., Sasao, T., & Wylde, R. 2008, Int. J. Infrared Millimeter Waves, 29, 69

Heiles, C., Perillat, P., Nolan, M., Lorimer, D., Bhat, R., Chosh, T., Howell, E., Lewis, M., et al. 2001, PASP, 113, 1247

Jung, T., Sohn, B. W., Kobayashi, H., Sasao, T., Hirota, T., Kameya, O., Choi, Y. K., & Chung, H. S. 2011, PASJ, 63, 375

Kim, H.-G., Han, S.-T., Sohn, B. W., Oh, S.-J., Je, D.-H., Wi, S.-O., & Song, M.-G. 2004, Proc. 7th Symp. European VLBI Network, ed. R. Bachiller, F. Colomer, J. J. Desmurs, P. de Vicente (Toledo: OAN), 281

Kim, J., Cho, S.-H., Oh, C. S., & Byun, D.-Y. 2010, ApJS, 188, 209

Kim, K.-T., Byun, D.-Y., Je, D.-H., Wi, S.-O., Bae, J.-H., Jung, T.-H., Lee, C.-H., Han, S.-T., et al. 2011, J. Korean Astron. Soc., 44, 81

Koo, B.-C., Park, Y.-S., Hong, S. S., Yun, H.-S., Lee, S.-G., Byun, D.-Y., Lee, J.-W., Choi, H.-K., et al. 2003, J. Korean Astron. Soc., 36, 43

Linsky, J. L. 1973, ApJS, 25, 163

Mangum, J. G. 1993, PASP, 105, 117

Middelberg, E., Roy, A. L., Walker, R. C., & Falcke, H. 2005, A&A, 433, 897

Oh, S.-J., Roh, D.-G., Wajima, K., Kawaguchi, N., Byun, D.-Y., Yeom, J.-H., Je, D.-H., & Han, S.-T. 2011, PASJ, in press

Page, L., Barnes, C., Hinshaw, G., Spergel, D. N., Weiland, J. L., Wollack, E., Bennett, C. L., Halpern, M., et al. 2003, ApJS, 148, 39

Roh, D.-G., & Jung, J. H. 1999, J. Korean Astron. Soc, 14, 123

Rohlfs, K., & Wilson, T. L. 2000, Tools of Radio Astronomy (New York: Springer)

Schloerb, F. P., & Snell, R. L. 1980, FCRAO Report 150 (Amherst: FCRAO)

Ulich, B. L., & Haas, R. W. 1976, ApJS, 30, 247

Wajima, K., Kim, H.-G., Han, S.-T., Roh, D.-G., Je, D.-H., Oh, S.-J., Wi, S.-O, & Korean VLBI Network Group 2005, preprint (arXiv:astro-ph/0511065)